

ORIGINAL ARTICLE

Nanoporous polystyrene prepared via the selective removal of the low M_w component in polystyrene blends

Fan-Yen Lin¹, Chad Daley¹, Jeremy Flannery¹, Sonia Zhang¹, Yu Chai¹ and James A Forrest^{1,2}

Herein, we report a straightforward technique for the creation of nanoporous polystyrene (PS) films. By preparing PS blend samples with M_w s of 600 000 and 600 g mol⁻¹ followed by rinsing with n-heptane, the low M_w component was dissolved and removed to afford a low-density network of high M_w PS. Nanoscale pores are formed as a result of the miscibility and stability of the initial state. The resulting materials were characterized using ellipsometry, atomic force microscopy and scanning electron microscopy. Materials with an effective refractive index as low as 1.1 can be prepared using this approach. The effects of varying the size of the low M_w polymer and the application of low friction surfaces prepared with the nanoporous samples were investigated.

Polymer Journal (2016) 48, 983–990; doi:10.1038/pj.2016.68; published online 31 August 2016

INTRODUCTION

The intrinsically high surface area associated with the internal structure of nanoporous materials endows these materials with a number of desirable properties that, in many cases, can be tuned by varying the degree of porosity. Therefore, nanoporous materials find use in a number of real-world applications including thermal insulation, optical coatings,¹ gas separation²/storage³ and chemical adsorption.^{4,5} Traditional methods for their preparation include templating⁶/lithographic techniques,^{7,8} the sol–gel method for creation of (extremely) low-density aerogels⁹ and leaching methods.¹⁰ Among these methods, leaching techniques are the most straightforward in their approach but are typically restricted to the use of immiscible materials due to the requirement that a single liquid (solvent) that is a solvent for one component cannot be a non-solvent for the other component. This restriction on immiscible materials leads to porous structures with pore sizes that are determined by the characteristic domain size of microscopic phase separation. A noteworthy exception is block copolymers where immiscible polymer species are grafted to one another through chemical bonds. In this case, the pore sizes are determined by the ordered structure of the copolymers (lamella, cylinder and gyroid), which have domain sizes comparable to the size of the chain.¹¹ The extensive use of block copolymers is limited by their high production costs, and the process involves the destruction of chemical bonds and is not as simple as straightforward leaching methods.

Herein, we describe a novel method for the creation of nanoporous polystyrene (PS) films. The technique exploits the relatively high entropic gain of short chains compared with that of long chains upon dissolution. We choose a solvent where the enthalpic contributions to

dissolution are (weakly) unfavorable. Entropic considerations allow for the dissolution of short chains while the long chains remain insoluble. We demonstrate that the morphologies can be tuned by the volume fraction and molecular weight of the low M_w components. In addition, the formation mechanism of the nanoporous structures is explained by the phase inversion model. The nanoporous films can be further combined with chemicals (for example, lubricating oil) to extend their application.

EXPERIMENTAL PROCEDURE

Materials and sample preparation

The polymers used in this study included monodisperse PSs of various different molecular weights (Table 1). First, each PS was dissolved in toluene (HPLC grade, Sigma-Aldrich, St Louis, MO, USA) to prepare PS/toluene solutions with concentrations ranging from 0.5 to 4 wt%. Second, the PS blend solutions were prepared by mixing low M_w and high M_w PS solutions with a low M_w PS solution with a volume fraction (ϕ) ranging from 0.1 to 0.9. The substrate was a silicon wafer (University Wafer Inc., South Boston, MA, USA, <100> orientation) with the native oxide intact, and this substrate was pre-cut into pieces that were 1 cm × 1 cm in size. Before spin-coating, the pre-cut silicon wafer pieces were rinsed and spin-washed using toluene at least five times.

The PS blend solutions were spin-coated onto pre-cut silicon wafer pieces at a speed of 2500 r.p.m. To avoid potential complications involving segregation of low M_w chains to the free air interface,¹² measurements on the as-cast films were performed without prior annealing.

Nanoporous films were prepared by submerging the as-cast films into a 20-ml vial full of n-heptane (HPLC grade, Sigma-Aldrich) for 60 s to dissolve the low M_w PS. After 60 s in the n-heptane bath, the films were removed and rinsed gently with n-heptane five times to remove any low M_w PS that remained in the films. Then, the films were dried using a slow stream of dry

¹Department of Physics and Astronomy, University of Waterloo, Waterloo, ON, Canada and ²Perimeter Institute for Theoretical Physics, Waterloo, ON, Canada
Correspondence: Professor JA Forrest, Department of Physics and Astronomy, University of Waterloo, 200 University Ave W, Waterloo, Ontario, Canada N2L 3G1.
E-mail: jforrest@uwaterloo.ca

Received 13 April 2016; revised 2 June 2016; accepted 3 June 2016; published online 31 August 2016

Table 1 Molecular weight and polydispersity for PS samples

M_w (g mol^{-1})	M_w/M_n
600	1.2
1140	1.2
1400	1.08
1850	1.16
2100	1.15
2500	1.09
3000	1.09
600K	1.10

Abbreviation: PS, polystyrene.
All the PS was obtained from Polymer Source Inc.

N_2 gas. The vials with 20 ml of n-heptane were discarded and replaced after being used for five films to limit the build-up of low M_w PS in the heptane bath. It is important to note that variations on this procedure (that is, thickness of blend film, volume of solvent and immersion time) do not result in strong variations in the observed morphology.

To prepare slippery surfaces from nanoporous films, the nanoporous film was prepared on top of the silicon wafer. Then, the lubricating oil was added to the surface of the nanoporous film, and the substrate was tilted to remove excess lubrication oil. Some of the lubrication oil becomes trapped by the nanoporous structure and forms a stable layer. The mass of the substrate was recorded before and after the addition of the lubricating oil to calculate the amount of lubricating oil per area. The lubricating oil was a perfluorinated fluid (that is, DuPont Krytox 100, Dupont, Wilmington, DE, USA, density = 1.87 g ml^{-1} at 0°C , kinematic viscosity = $0.12 \text{ cm}^2 \text{ s}^{-1}$ at 20°C).

Methods

Raman spectroscopy. For this measurement, the high M_w polymer that was mentioned above was substituted with a high M_w fully deuterated (d8) chain (PS, $M_w = 627\,000 \text{ g mol}^{-1}$, PDI = 1.09). To separate the substrate contributions from the Raman signal of the polymer, quartz windows were used rather than silicon wafers. Aside from these distinctions, which have no effect on the leaching process, the sample preparation was the same as that described above. The Raman spectra were acquired using a Horiba Jobin Yvon HR800 series spectrometer (Horiba, Kyoto, Japan) with an excitation wavelength of 532 nm and a spectral resolution of 0.4 cm^{-1} .

Quartz crystal microbalance. The Quartz crystal microbalance (QCM) measurements were carried out using a Q-Sense D300 system that was equipped with an axial flow chamber (QAF302, Q-Sense, Stockholm, Sweden) and an Au sensor (Q-Sense). The PS blend solutions consisted of 600 g mol^{-1} mixed with $600\text{K} \text{ g mol}^{-1}$ (600/600K) with a ϕ value ranging from 0.1 to 0.9 were spin-coated onto the QCM sensors, resulting in an $\sim 180\text{-nm}$ -thick 600/600K PS blend film on the top of each sensor. The solvent volume in the chamber above the film was $100 \mu\text{l}$. The mass change in the PS blend film that was on the top of the sensor was calculated using the Sauerbrey equation:¹³ $\Delta m = -C\Delta f$, where C is the constant ($C = 17.7 \text{ ng Hz}^{-1} \text{ cm}^{-2}$) for the 5 MHz sensor crystal. The leached mass was determined *in situ* by the Δf that resulted in a new stable plateau (that is, the frequency no longer changes). Therefore, the measurement time was not limited to the 1 min leaching time used for the samples described above.

Ellipsometry. Nulling ellipsometry (Exacta 2000 self-nulling ellipsometer; Waterloo Digital Electronics, Waterloo, ON, Canada) was used to measure the optical properties of the nanoporous films. Six or more PS blend films were prepared for each volume fraction with a range of thickness (that is, 30–300 nm) by varying the concentration of the PS blend solutions from 0.5 to 4 wt%. For a single film, the ellipsometry measurement provides two zone-averaged angles (that is, polarizer (P) and analyzer (A)), which are calculated from a simple model using the film thickness and index of refraction. To unequivocally determine the index of refraction for a given volume fraction, P and A are required from films of varying thicknesses (that is, ideally over a wide

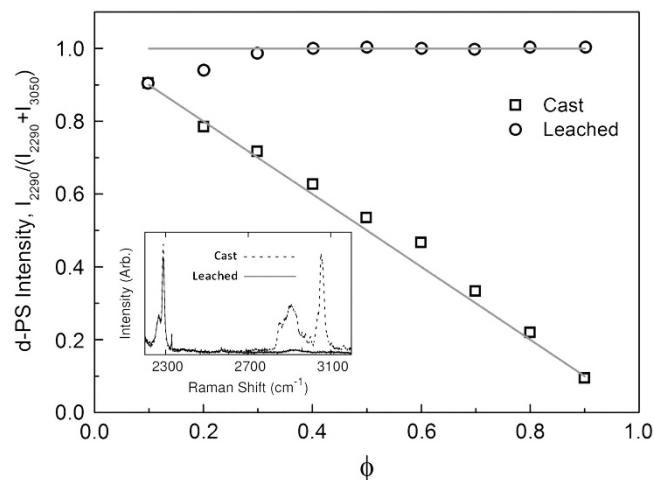


Figure 1 Deuterated (high M_w) peak intensity normalized to the sum of the deuterated/hydrogenated peak intensities as a function of the low M_w polystyrene (PS) volume fraction (ϕ) for the cast (squares) and leached (circles) samples. The solid lines indicate ideal behaviors. Inset: Example Raman spectra taken for a single ($\phi = 0.5$) sample before and after leaching. The hydrogenated-PS peak is located at 3050 cm^{-1} , and deuteration shifts this peak to 2290 cm^{-1} . A full color version of this figure is available at *Polymer Journal* online.^{14,16,17}

range of thickness). The single value of the refractive index that best describes all P and A values for a given volume fraction is the index of refraction for that volume fraction.

Microscopy techniques. Atomic force microscopy (AFM, JPK Nanowizard 3, JPK, Berlin, Germany) and scanning electron microscopy (SEM, Zeiss Merlin and ULTRA plus, Zeiss, Oberkochen, Germany) were employed to investigate the surface morphologies (AFM) and cross-sectional structures (SEM). For the SEM sample, a bare silicon wafer was scored on the non-polished side before preparing the sample. After the nanoporous film was prepared on top of the silicon wafer, the sample was immersed in liquid nitrogen. Then, the sample was removed from the liquid nitrogen and cleaved along the scratch line.

RESULTS AND DISCUSSION

We investigated the efficiency of the leaching process using two approaches. First, selective deuteration and Raman spectroscopy were employed to determine the efficiency of the leaching process. Deuteration of the high M_w chains shifts their characteristic Raman peaks relative to the non-deuterated chains and provides a method of spectroscopic contrast between the low and high M_w species. In particular, the peak located at 3050 cm^{-1} in normal PS (associated with phenyl C-H stretch^{14,15}) shifted to 2290 cm^{-1} upon deuteration. The relative intensities of these two peaks provide a measure of the relative amounts of the high and low M_w materials. The intensity of the deuterated signal at 2290 cm^{-1} normalized to the combined intensities of the 2290 and 3050 cm^{-1} peaks is shown (Figure 1). The as-cast films exhibited a straight line with a slope of 1, as expected. For the leached films, the hydrogenated component was not observed in the Raman spectra for ϕ larger than 0.3 (see inset for the case of $\phi = 0.5$). However, for a low ϕ of 0.2 and 0.3, a reduced leaching efficiency was observed, and for $\phi = 0.1$, no detectable change in the relative intensities of the deuterated/hydrogenated components was observed. Therefore, the low M_w PS at such a low ϕ is not as easily leached out in the 1 min time frame used for the sample preparation as it is at higher volume fractions.

A second technique to measure the leaching efficiency involves direct mass loss detection with the QCM. QCM is a straightforward

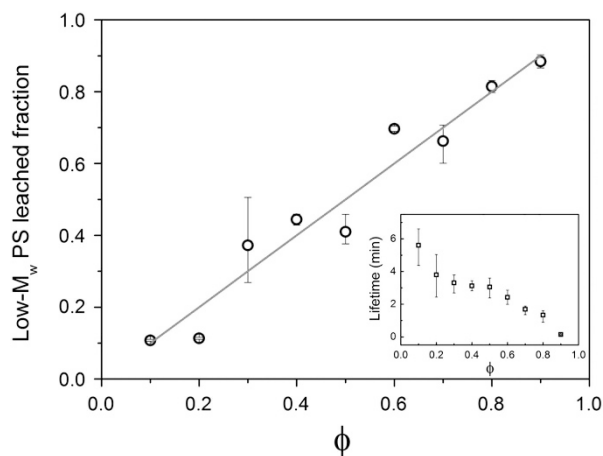


Figure 2 Leached fraction of low M_w polystyrene (PS) from the 600/600K PS blend films measured by Quartz crystal microbalance (QCM) as a function of the low M_w PS volume fraction (ϕ) (open circle). The red solid line represents the ideal leached fraction of low M_w PS. A full color version of this figure is available at *Polymer Journal* online.

method for measuring the efficiency of the leaching process (Figure 2). In this case, the contrast between the low and high M_w s is provided by their differential solubility in n-heptane. Upon exposure to n-heptane, the low M_w component of the PS blend film dissolves, and the resulting mass of the PS film changes. This mass change can be directly monitored by the change in the resonance frequency of the QCM sensor. The low M_w PS leached fraction can be determined by combining the bulk PS density of 1.05 g ml^{-1} ,¹⁸ the thickness of the PS blend film before leaching, and the mass change in the PS blend film after leaching. The low M_w PS leached fraction increases with increasing ϕ and follows the trend of the ideal leached fraction. Therefore, n-heptane can penetrate into the PS blend film to dissolve the low M_w PS. An interesting difference was observed between these two measures of the leaching efficiency. For the *ex situ* films measured using Raman spectroscopy, less than ideal leaching efficiency was obtained for low values of ϕ but the QCM measurements indicate ideal efficiency over the entire range of ϕ . This difference can be explained by examining the dissolution kinetics. The inset of Figure 2 shows the average lifetime for the dissolution of the low M_w component as a function of ϕ . For smaller values of ϕ , the lifetime is significantly larger than the 1 min time used in the first method.

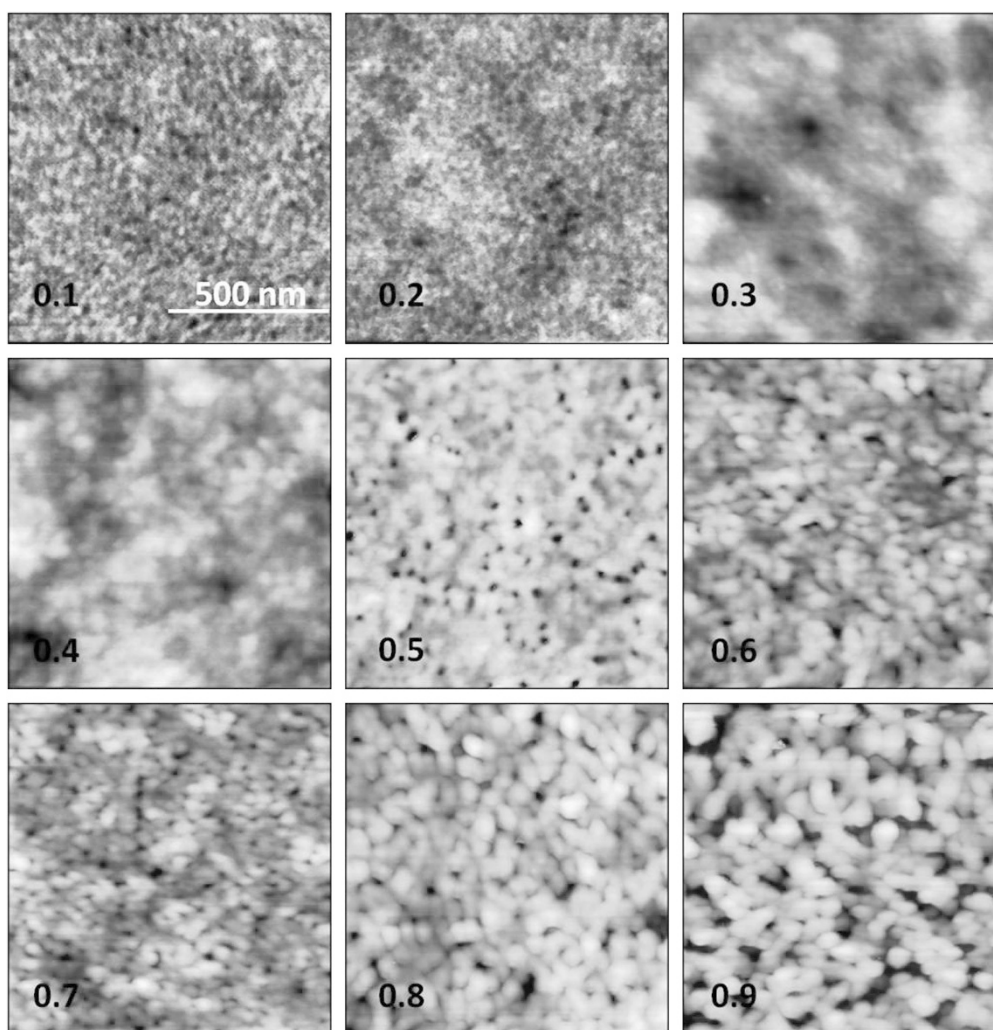


Figure 3 Atomic force microscopy (AFM) measurements indicating that the surface morphology of the polystyrene (PS) blend films (600/600K) changed after leaching as a function of volume fraction (ϕ). The size of each topography image is $1 \mu\text{m} \times 1 \mu\text{m}$. A full color version of this figure is available at *Polymer Journal* online.

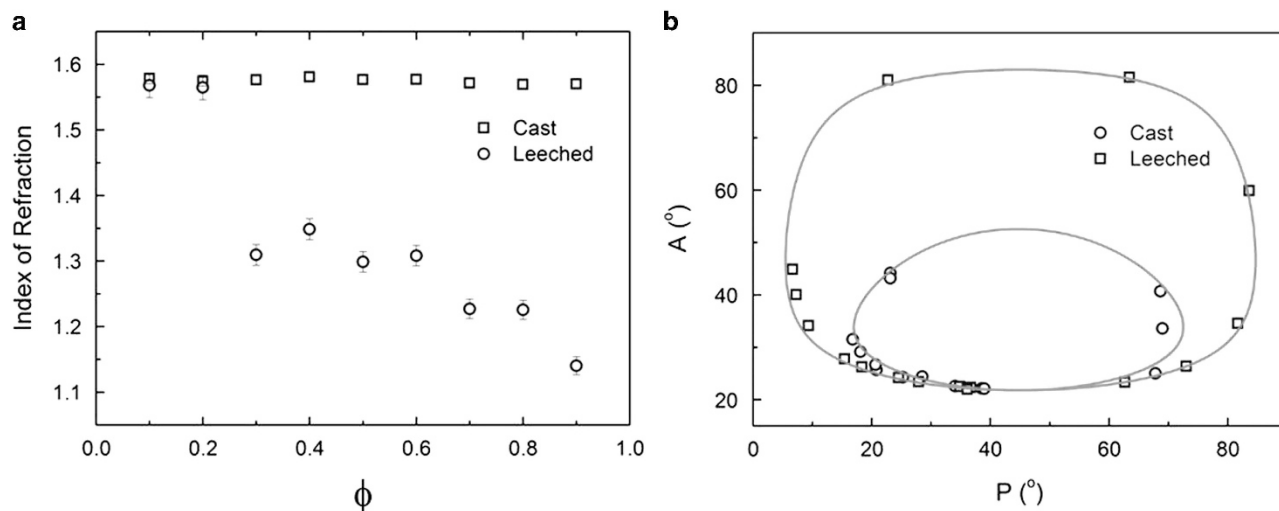


Figure 4 (a) Index of refraction for the cast and leached polystyrene (PS) films as a function of the low M_w PS volume fraction (ϕ). (b) Raw data measured using ellipsometry for the cast and leached films with $\phi=0.5$ in a 600/600K PS blend. The red solid lines are fitted using a three-layer model (i.e., silicon wafer/ SiO_2 /PS). A full color version of this figure is available at *Polymer Journal* online.

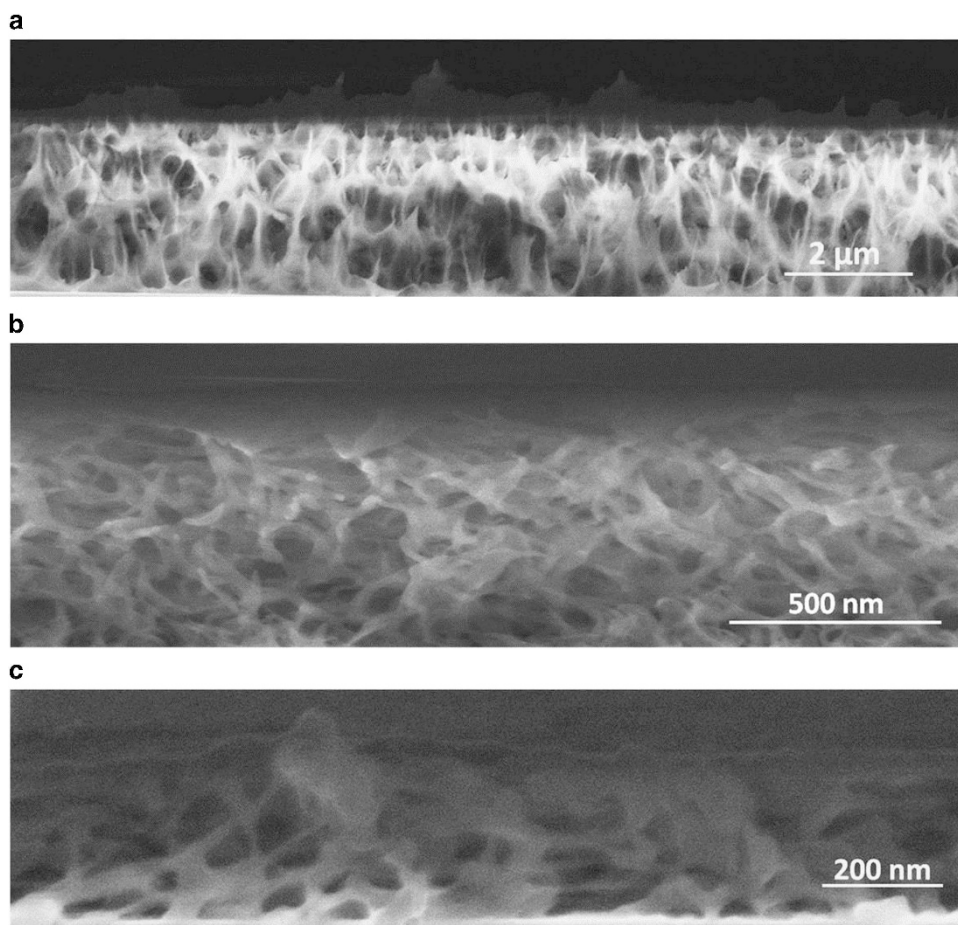


Figure 5 Cross-sectional scanning electron microscopy (SEM) images recorded after leaching for a ϕ value of (a) 0.2, (b) 0.5 and (c) 0.8 in the blend consisting of 600/600K polystyrene (PS) films.

Therefore, the blend samples in Figure 1 are not exposed to n-heptane sufficiently long for complete dissolution of the low M_w component.

The AFM images (Figure 3) show the surface morphologies with increasing ϕ values. All these surface structures exhibit significant

differences from a clean PS surface. In all cases, the surface appears porous but with no monotonic changes in the structure observed as ϕ changes. Although AFM provides a wealth of information regarding the surface structure of the film, it provides little to no information on

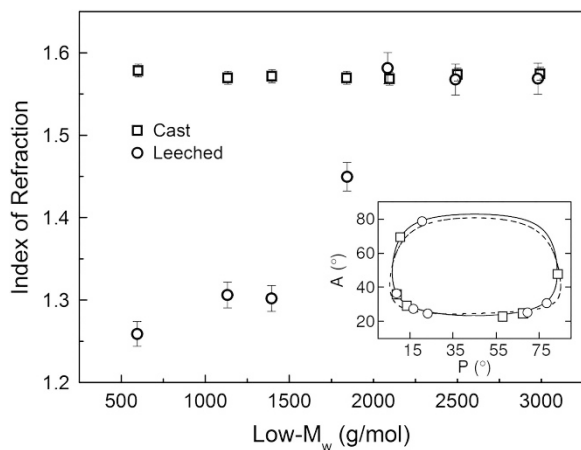


Figure 6 Index of refraction for the cast and leached polystyrene (PS) films as a function of a lower molecular weight. In all cases, the films were prepared with a ϕ value of 0.5. Inset: Raw ellipsometric data for $M_w = 2500 \text{ g mol}^{-1}$ in the cast and leached films. The solid line represents a uniform film with an index of refraction of 1.57, and the dashed line represents the four-layer model (i.e., silicon wafer/SiO₂/porous PS/dense PS layer).

the depth, extent or connectivity of the internal porous structures. However, the pore structure does appear on a length scale that is much smaller than the wavelength of optical light. This result suggests that we should observe specular reflection rather than scattering of light; therefore, ellipsometric techniques can be employed.

The average index of refraction of the film can be determined using ellipsometry. From the index of refraction, the Lorentz–Lorenz relationship (Equation 1) can be used to calculate the average density of the film and infer the amount of free space in the internal structure. Here, ρ is the density and n is the index of refraction. All ellipsometric measurements were performed within the context of an approximation where we assume that the film has a uniform thickness and uniform refractive index. In practice, this assumption will hold for internal structures on a length scale that is significantly smaller than the wavelength used in this study (that is, 633 nm).

$$\rho \propto \frac{n^2 - 1}{n^2 + 2} \quad (1)$$

In Figure 4a, the measured index of refraction is plotted as a function of ϕ for both the cast and leached films. For all ϕ , the cast films are described by a single value of the index of refraction (that is, ~ 1.57). Because no porous structures formed inside the cast films, the average densities are the same as that of neat PS and exhibit the same index of refraction. For the leached films, the index of refraction decreased with increasing ϕ , which indicates that the average density decreased. In the simplest picture, when the low M_w PS is leached from the PS blend, the volume that had been occupied by the low M_w PS is replaced by air, which results in the formation of porous structures. The details of the pore shapes and sizes are determined by the diffusive processes that occur while the film is immersed in heptane. As a result of this decrease in the density and refractive index, the measured P and A values of the leached film will exhibit significantly different behavior from that of the cast film (Figure 4b). In particular, for $\phi > 0.3$, significant changes in the apparent refractive index were observed. Notably, for the highest volume fraction (that is, $\phi = 0.9$), the refractive index was only $n = 1.15$. In addition, these highly porous structures can be quite fragile. For example, after submerging the cast film into the n-heptane bath, the film should

be gently rinsed with the n-heptane. If the sample is spin-washed at high speeds, the porous structures collapse.

Although AFM can determine the surface structure on small length scales and ellipsometry provides insight into properties averaged over large length scales, neither of these techniques is able to provide details regarding the nature of the pores throughout the sample. SEM was used to investigate and compare the leached films at $\phi = 0.2, 0.5$ and 0.8 (Figure 5). As previously mentioned, the samples used for the SEM studies were cleaved to provide a real cross-sectional image of the nanoporous sample. Based on the cross-sectional SEM images (Figure 5), porous structures were formed in all the leached films for $\phi = 0.2, 0.5$ and 0.8 . The average size of the pores decreased as ϕ increased. The porous structures for $\phi = 0.5$ and 0.8 were more uniform than the porous structures at $\phi = 0.2$. For the film with $\phi = 0.2$, pores with size greater than $1 \mu\text{m}$ were observed. For samples with these pores, any incident light was strongly scattered. Therefore, in this case, ellipsometry is not a useful tool for investigating the film properly, and the same index of refraction for the cast and leached films is obtained. In addition, the reduced leaching efficiency (Figure 1) at low ϕ does not completely inhibit the formation of nanoporous structures (Figure 5a). As ϕ increased, the size of the pores decreased, and for $\phi = 0.8$, the pores were $\sim 100 \text{ nm}$ in size.

The solubility of PS in n-heptane strongly depends on the M_w of the polymer. This may have a significant impact on the ability of these binary blends to form nanoporous structures. Therefore, we investigated the effect of varying the molecular weight of the low M_w component (Figure 6) while maintaining a fixed volume fraction at $\phi = 0.5$. These samples were studied with ellipsometry in the same manner as those in Figure 4, where multiple films over a range of thickness were used to determine the refractive index of the nanoporous material. For each M_w , these measurements were performed on both the as-cast and leached films. The resulting measured P and A values were used to calculate the refractive index of that particular blend. As expected, the indices of refraction for all the as-cast films were consistent with that of bulk PS. Leached films with low $M_w < 2000 \text{ g mol}^{-1}$ possessed a refractive index of ~ 1.3 . At a M_w of $\sim 2000 \text{ g mol}^{-1}$, the apparent refractive index abruptly changes to the bulk value. Analogous to the case for small ϕ , which also exhibits a bulk-like apparent refractive index, SEM was employed to study the samples. The cross-sectional SEM images (Figure 7) show a dense layer near the free surface which is gradually formed with the molecular weight of low M_w component increasing and the rest of the films with pores, some of them larger than $1 \mu\text{m}$. For the 2500/600K PS blend films, both the dense layer and porous structure layer with a thickness of $\sim 100 \text{ nm}$ were observed in the leached film (Figure 7c). The four-layer model (that is, silicon wafer/SiO₂/porous PS/dense PS layer) consisted of a 100-nm-thick dense layer with a refractive index of 1.57 and a porous layer with a refractive index of 1.30, and a varying thickness was applied to simulate the ellipsometric results. The model with an additional dense layer exhibited a similar refractive index as that of the bulk PS in the leached film (that is, 2500/600K) (Figure 6, inset). Therefore, the porous microstructures prevent the use of ellipsometry. In the first case, for micron size pores, the amount of scattering may lead to unreliable ellipsometry measurements. Second, even if ellipsometry measurements were possible, modeling indicated that it may not be possible to distinguish between a porous layer with a bulk-like coating and a simple bulk-like film (with a smaller thickness).

In the preceding sections, we introduced a simple method for the creation of nanoporous PS films and characterized the resulting structures. This technique exploits the much larger entropic gain for

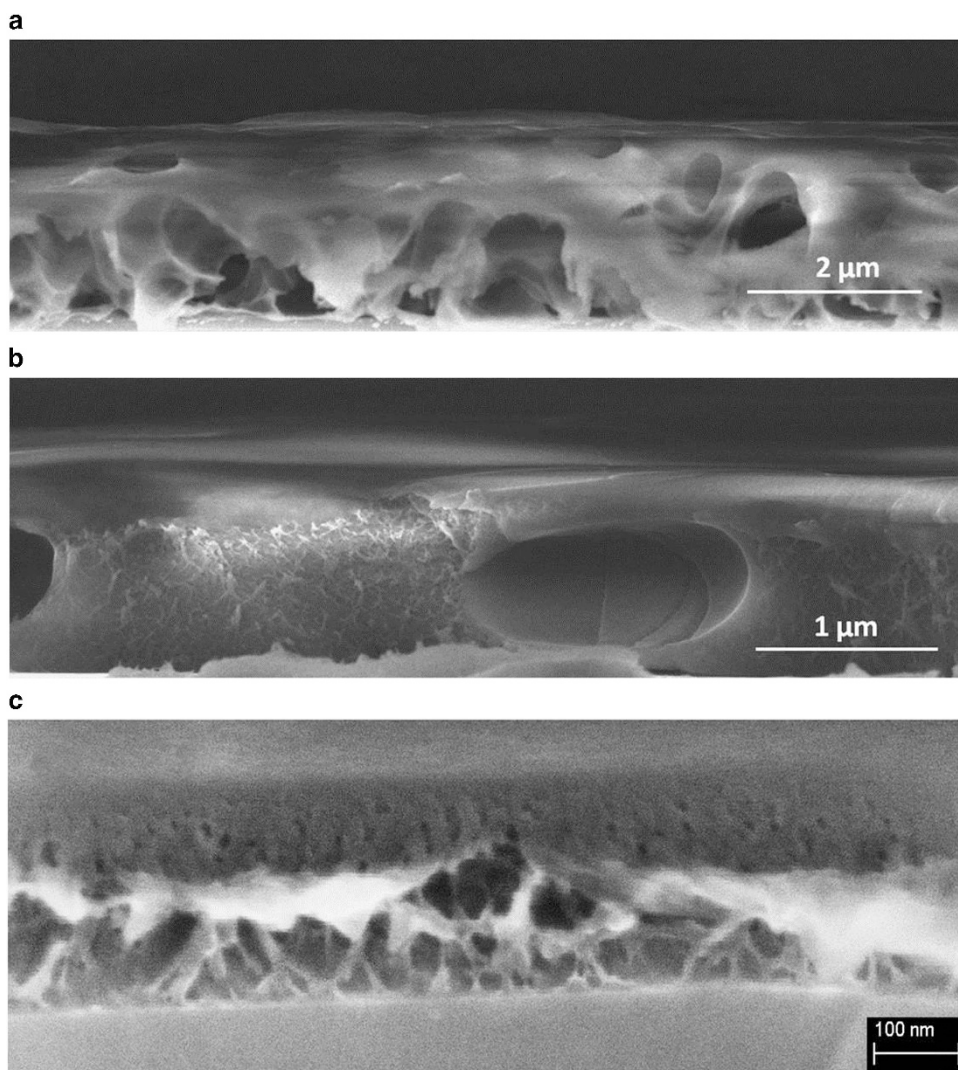


Figure 7 Cross-sectional scanning electron microscopy (SEM) images recorded after leaching for ϕ of 0.5 in a blend with (a) 1400/600K, (b) 2100/600K and (c) 2500/600K polystyrene (PS) films, respectively.

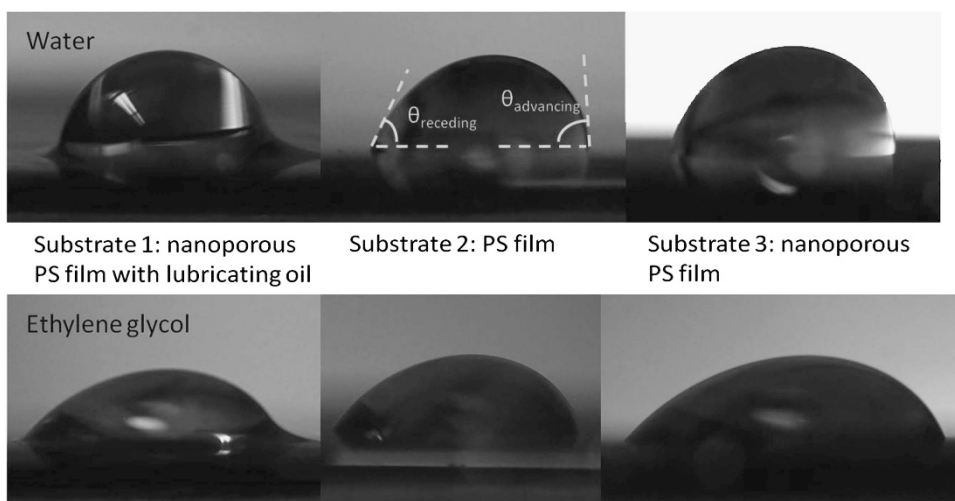


Figure 8 Optical images demonstrate the advancing and receding contact angles for the drops of water (top layer) and ethylene glycol (bottom layer) sliding on three different substrates. The advancing and receding contact angles are measured by tilting the substrate until the liquid drop exhibits obvious motion. A full color version of this figure is available at *Polymer Journal* online.

Table 2 Contact angle hysteresis of water and ethylene glycol on three different substrates obtained from the difference between the advancing and receding contact angles measured in Figure 8

Drop liquid	Substrate 1	Substrate 2	Substrate 3
Water	<3°	25°	18°
Ethylene glycol	9°	27°	17°

The error bar for the contact angle hysteresis is $\pm 2^\circ$.

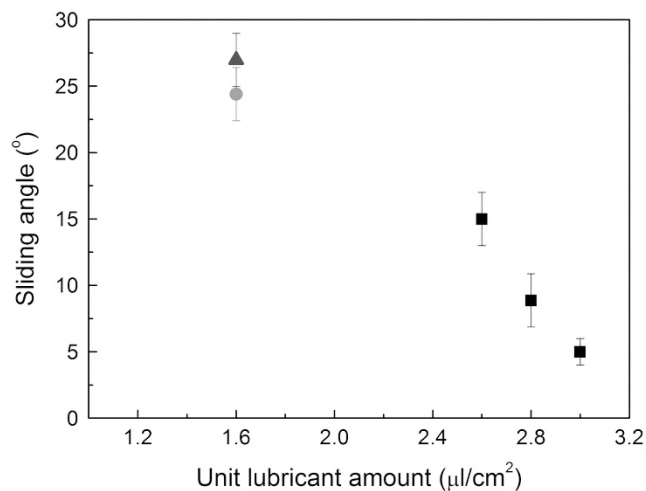


Figure 9 Sliding angle as a function of the unit lubrication amount (i.e., the thickness of the lubricating oil) for silicon oil (black square, $6\ \mu\text{l}$, $20.4\ \text{mN m}^{-1}$), water (red circle, $10\ \mu\text{l}$, $72.4\ \text{mN m}^{-1}$) and ethylene glycol (blue triangle, $10\ \mu\text{l}$, $48.1\ \text{mN m}^{-1}$). In comparison with the effect of the unit lubricant amount, the volume of the drop or the surface tension of the test liquid affects the sliding angle by approximately $\pm 1^\circ$ and is considered negligible. The data for silicon oil were obtained from the literature. A full color version of this figure is available at *Polymer Journal* online.²⁷

the dissolution of short chains relative to long chains. By choosing an initial blend system consisting of low and high M_w PSs, our initial system was completely miscible and stable under ambient conditions. By subsequently exposure to a weakly unfavorable solvent (that is, n-heptane), the low M_w material was removed from the system, leaving behind a porous high M_w film. The method can be generally classified as a leaching technique for producing porous systems. The novel aspect of this technique is that the initial system is miscible and stable, and nanoscale pores are found as a result. The technique is similar to phase inversion methods that are commonly used for the production of gas separation membranes.^{19,20} There, the underlying principle is to induce microphase separation upon exposure of a polymer/solvent film to a non-solvent. Depending upon the relative volatilities, (non)solvent quality and details of the non-solvent exposure, a range of porous structures can be produced.^{21,22} In fact, extensive theoretical studies have been focused on understanding the processes that lead to pore formation in phase inversion processes.^{23,24} In particular, Cohen *et al.*²⁴ developed a diffusion-based model considering the flux of solvent/non-solvent molecules upon immersion of a polymer/solvent film in a non-solvent bath. As the concentration gradient of the solvent/non-solvent molecules equilibrates, the system moves along a trajectory within the polymer/solvent/non-solvent ternary phase space. Upon crossing the spinodal line, a single-phase system is no longer stable, and phase separation spontaneously occurs, leading to pore formation. Our

system is the same in principle, with stable low M_w chains serving as the solvent component and n-heptane acting as the non-solvent.

As an example of the general applicability of nanoporous polymers and a test of this particular process, we investigated the formation of 'slippery surfaces'. In general, two factors are employed to characterize slippery surfaces including (1) a very low contact angle hysteresis, which is the difference between the advancing and receding contact angles and (2) a very low sliding angle, which is the surface tilt required for drop motion.^{25,26} The contact angle hysteresis of water and ethylene glycol droplets is much smaller on our slippery surface (substrate 1) than that on substrates 2 and 3 (Figure 8 and Table 2). The results in Figure 9 indicate that the droplet sliding angle on our slippery surface follows the trend of unit lubricant amount dependent sliding angle reported in the literature.²⁷ These results demonstrate the nanoporous film can trap the lubricating oil and form a slippery surface.^{25,26}

In summary, we demonstrated that our novel method can easily provide nanoporous structures for most volume fraction (ϕ) values in a short period of time. The effective material properties due to the porosity of the nanoporous films were investigated using ellipsometry and discussed in terms of the index of refraction. As the value of ϕ increased, the index of refraction decreased and reached a value as low as 1.1 for the high ϕ samples. The morphologies of the internal structures can be tuned by changing the ϕ or the molecular weight of the low M_w component. The as-prepared nanoporous films can be treated with lubricating oil to form 'slippery surfaces'. Although we have presented the technique using PS/n-heptane, we believe our approach can be applied to almost any polymer system for which a solvent can be found for the low M_w version, which is a non-solvent for the same polymer at high M_w .

CONFLICT OF INTEREST

The authors declare no conflict of interest.

ACKNOWLEDGEMENTS

Financial support from the Natural Sciences and Research Council of Canada is gratefully acknowledged. The research at the Perimeter Institute is supported by the Government of Canada through Industry Canada and the Province of Ontario through the Ministry of Economic Development and Innovation. JAF is grateful for the funding provided by the Paris Sciences Chair of the ESPCI, Paris, France.

- 1 Foss, C. A., Hornyak, G. L., Stockert, J. A. & Martin, C. R. Optical-properties of composite membranes containing arrays of nanoscopic gold cylinders. *J. Phys. Chem.* **96**, 7497–7499 (1992).
- 2 de Vos, R. M. & Verweij, H. High-selectivity, high-flux silica membranes for gas separation. *Science* **279**, 1710–1711 (1998).
- 3 Germain, J., Fréchet, J. M. J. & Svec, F. Nanoporous polymers for hydrogen storage. *Small* **5**, 1098–1111 (2009).
- 4 Schneider, K. & van Gassel, T. J. Membrandestillation. *Chemie Ing. Tech.* **56**, 514–521 (1984).
- 5 Eustache, H. & Histi, G. Separation of aqueous organic mixtures by pervaporation and analysis by mass spectrometry or a coupled gas chromatograph-mass spectrometer. *J. Memb. Sci.* **8**, 105–114 (1981).
- 6 Hulteen, J. C. & Martin, C. R. A general template-based method for the preparation of nanomaterials. *J. Mater. Chem.* **7**, 1075–1087 (1997).
- 7 Chu, S.-Z., Wada, K., Inoue, S., Isogai, M. & Yasumori, A. Inside Front Cover: Fabrication of Ideally Ordered Nanoporous Alumina Films and Integrated Alumina Nanotubule Arrays by High-Field Anodization (Adv. Mater. 17/2005). *Adv. Mater.* **17**, 2115–2119 (2005).
- 8 Lee, W., Ji, R., Gösele, U. & Nielsch, K. Fast fabrication of long-range ordered porous alumina membranes by hard anodization. *Nat. Mater.* **5**, 741–747 (2006).
- 9 Tillotson, T. M. & Hrubesh, L. W. Transparent ultralow-density silica aerogels prepared by a two-step sol-gel process. *J. Non Cryst. Solids* **145**, 44–50 (1992).

- 10 Lee, J., Hiraio, A. & Nakahama, S. Polymerization of monomers containing functional silyl groups. 5. Synthesis of new porous membranes with functional groups. *Macromolecules* **21**, 274–276 (1988).
- 11 Zhao, D., Feng, J., Huo, Q., Melosh, N., Fredrickson, G., Chmelka, B. & Stucky, G. Triblock copolymer syntheses of mesoporous silica with periodic 50 to 300 angstrom pores. *Science* **279**, 548–552 (1998).
- 12 Hariharan, A., Kumar, S. K. & Russell, T. P. A lattice model for the surface segregation of polymer chains due to molecular weight effects. *Macromolecules* **23**, 3584–3592 (1990).
- 13 Sauerbrey, G. Verwendung von Schwingquarzen zur Wagungdiinner Schichten und zur Mikrowagung. *Z. Phys.* **155**, 206–222 (1959).
- 14 Köhler, A., Khan, A. L. T., Wilson, J. S., Dosche, C., Al-Suti, M. K., Shah, H. H. & Khan, M. S. The role of C-H and C-C stretching modes in the intrinsic non-radiative decay of triplet states in a Pt-containing conjugated phenylene ethynylene. *J. Chem. Phys.* **136** (2012).
- 15 Holinga, G. J., York, R. L., Onorato, R. M., Thompson, C. M., Webb, N. E., Yoon, A. P. & Somorjai, G. A. An SFG study of interfacial amino acids at the hydrophilic SiO₂ and hydrophobic deuterated polystyrene surfaces. *J. Am. Chem. Soc.* **133**, 6243–6253 (2011).
- 16 Prystupa, D., Anderson, A. & Torrie, B. H. Raman and infrared study of solid benzyl alcohol. *J. Raman Spectrosc.* **25**, 175–182 (1994).
- 17 Bergner, G., Albert, C. R., Schiller, M., Bringmann, G., Schirmeister, T., Dietzek, B., Niebling, S., Schlücker, S. & Popp, J. Quantitative detection of C-deuterated drugs by CARS microscopy and Raman microspectroscopy. *Analyst* **136**, 3686–3693 (2011).
- 18 Brandrup, J. & Immergut, E. H. *Polymer Handbook* (John Wiley and Sons, New York, NY, USA, 1989).
- 19 Koros, W. J. & Fleming, G. K. Membrane-based gas separation. *J. Memb. Sci.* **83**, 1–80 (1993).
- 20 Guillen, G. R., Pan, Y., Li, M. & Hoek, E. M. V. Preparation and characterization of membranes formed by nonsolvent induced phase separation: a review. *Ind. Eng. Chem. Res.* **50**, 3798–3817 (2011).
- 21 Smolders, C. A., Reuvers, A. J., Boom, R. M. & Wienk, I. M. Microstructures in phase-inversion membranes. Part 1. Formation of macrovoids. *J. Memb. Sci.* **73**, 259–275 (1992).
- 22 Radovanovic, P., Thiel, S. W. & Hwang, S.-T. Formation of asymmetric polysulfone membranes by immersion precipitation. Part II. The effects of casting solution and gelation bath compositions on membrane structure and skin formation. *J. Memb. Sci.* **65**, 231–246 (1992).
- 23 Altena, F. W. & Smolders, C. A. Calculation of liquid liquid-phase separation in a ternary-system of a polymer in a mixture of a solvent and a nonsolvent. *Macromolecules* **15**, 1491–1497 (1982).
- 24 Cohen, C., Tanny, G. B. & Prager, S. Diffusion-controlled formation of porous structures in ternary polymer systems. *J. Polym. Sci. Polym. Phys. Ed.* **17**, 477–489 (1979).
- 25 Wong, T.-S., Kang, S. H., Tang, S. K. Y., Smythe, E. J., Hatton, B. D., Grinthal, A. & Aizenberg, J. Bioinspired self-repairing slippery surfaces with pressure-stable omniphobicity. *Nature* **477**, 443–447 (2011).
- 26 Chen, W., Fadeev, A. Y., Hsieh, M. C., Öner, D., Youngblood, J. & McCarthy, T. J. Ultrahydrophobic and ultralyophobic surfaces: some comments and examples. *Langmuir* **15**, 3395–3399 (1999).
- 27 Yao, X., Hu, Y., Grinthal, A., Wong, T.-S., Mahadevan, L. & Aizenberg, J. Adaptive fluid-infused porous films with tunable transparency and wettability. *Nat. Mater.* **12**, 529–534 (2013).